In situ radiographic investigation of lithiation and delithiation mechanisms in a Sn-electrode lithium ion battery[#]

Fu Sun,*[a, b] Henning Markötter, [a, b] Dong Zhou, [a, b] Saad Sabe Sulaiman Alrwashdeh, [a, b, c] Andre Hilger, [b] Nikolay Kardjilov, [b] Ingo Manke[b] and John Banhart [a, b]

[a] Fu Sun, Prof. Dr. John Banhart, Dr. Henning Markötter, Dong Zhou, Saad Sabe Sulaiman Alrwashdeh
Institute of Material Science and Technologies
Technical University Berlin
10623 Berlin, Germany
E-mails: fu.sun@helmholtz-berlin.de
john.banhart@tu-berlin.de

[b] Fu Sun, Dr. Henning Markötter, Dong Zhou, Saad Sabe Sulaiman Alrwashdeh, Dr. Andre Hilger, Dr. Nikolay Kardjilov, Dr. Ingo Manke and Prof. Dr. John Banhart
Helmholtz Centre Berlin for Materials and Energy
Hahn-Meitner-Platz 1
14109 Berlin, Germany

[c] Saad Sabe Alrwashdeh
Mechanical Engineering Department
Faculty of Engineering, Mu'tah University
P.O Box 7, Al-Karak 61710 Jordan

[#] manuscript published in Chemisty and Sustainability - ChemSusChem 9(9), 946–950 (2016)
Wiley, ISSN: 1864-564X — doi: 10.1002/cssc.201600220

The lithiation and delithiation mechanisms of multiple-Sn particles in a customized flat radiography cell were investigated by *in situ* synchrotron radiography. For the first time, four hitherto unknown de/lithiation phenomena in a Sn-electrode battery system are highlighted: 1 The de/lithiation behavior varies between different Sn particles; 2 The time required to lithiate individual Sn particle is markedly different from the time needed to discharge the complete battery; 3 Electrochemical deactivation of originally electrochemically active particles is reported; 4 A change of electrochemical behavior of individual particles during cycling is found and explained by dynamic changes of de/lithiation pathways amongst particles within the electrode. These unexpected findings fundamentaly expand the understanding of the underlying de/lithiation mechanisms inside commercial lithium ion batteries (LIBs) and would open new design principles for high-performance next-generation LIBs.

Lithium ion batteries (LIBs) are the dominant energy carrier in many applications ranging from portable electronics to hybrid electric vehicles.[1-4] The development of next-generation LIBs with superior energy and power density and long-term cycling stability necessitates a fundamental understanding of de/lithiation mechanisms inside battery systems. Currently, direct visualization into de/lithiation process has been largely provided by *in situ* transmission electron microscopy (TEM) investigations.[5, 6] However, Zhong *et al.* argue that the "end/point contact" architecture of active materials used in the *in situ* TEM technique may deviate from the commercial "flooding geometry" contacts and they find the multiple-stripe lithiation mechanism in a flooding geometry by investigating SnO_2 nanowires.[7] Furthermore,

Gu *et al.* suggest that the open-cell configuration and the ionic/Li_2O electrolyte are also inherently different from real commercial batteries and they have developed a sealed *operando* TEM electrochemical cell and found that the lithiation of Si nanowire immersed in the liquid electrolyte progresses in the core-shell fashion.[8] Previous work carried out based on the *in situ* TEM have provided insightful information into the structural and chemical evolution of electrodes during de/lithiation. Nevertheless, one typical deficiency associated with the *in situ* TEM studies is that they are limited to explore the de/lithiation mechanism on atomic or single nanowire/nanoparticle level only, missing the interplay amongst multiple particles and the interactions between active material and conductive/binder agent composite. Realistically, a commercial LIB electrode is an assembly of active particles, organic polymeric binder and conducting agent.[9] Thus, direct observation of the de/lithiation process on the multiple-particle scale can provide additionally realistic insights into the operation of LIBs and guide engineers designing the electrode architecture in developing more advanced next-generation LIBs.

Herein a cell suitable for *in situ* radiography was built and the de/lithiation process of multiple-Sn particles was investigated by synchrotron X-ray radiography. Some de/lithiation behaviors of Sn particles obtained from this *in situ* radiography cell are consistent with previous results.[8] However, contrary to the widespread belief that the lithium ions are proposed to diffuse uniformly from the separator to the current collector with the formation of an electrode-level de/lithiation front,[10] we find a number of phenomena in the battery systems that cast doubts on this belief. These unexpected findings, which cannot be obtained by the overall macroscopic electrochemical characterizations and a single-particle de/lithiation model, fundamentally expand our understanding of underlying de/lithiation mechanisms in practical commercial LIBs and would open new design principles and opportunities for high-performance next-generation LIBs.

The design of the *in situ* 2D radiography cell (radio-cell) and the schematic illustration of the synchrotron setup are illustrated in Figure 1a,c, along with a photograph of the radio-cell, Figure 1b. Figure SI of the SI (Supporting Information) shows a projection image of the Li electrode/separator/Sn electrode assembly within the cell obtained after the synchrotron X-ray measurements by using a laboratory micro X-ray source.[11] A weight-ratio of Sn:Carbon:Binder of 60:30:10 was used to prevent possible particle overlapping in the radiographs. More details of the cell and the measurement procedure are described in the experimental section and SI. After assembling the radio-cell, cyclic voltammetry (CV) was performed to verify the reduction and oxidation characteristics of Sn, as shown in Figure S2. The clearly observed anodic/cathodic peaks shown in SI Figure 2b are in good agreement with previously reported Sn/Carbon composite LIBs.[12] In a next step, the cell was dis/charged while conducting synchrotron X-ray radiography. Typical dis/charge curves shown in SI Figure 2a also agree with previous results.[13]

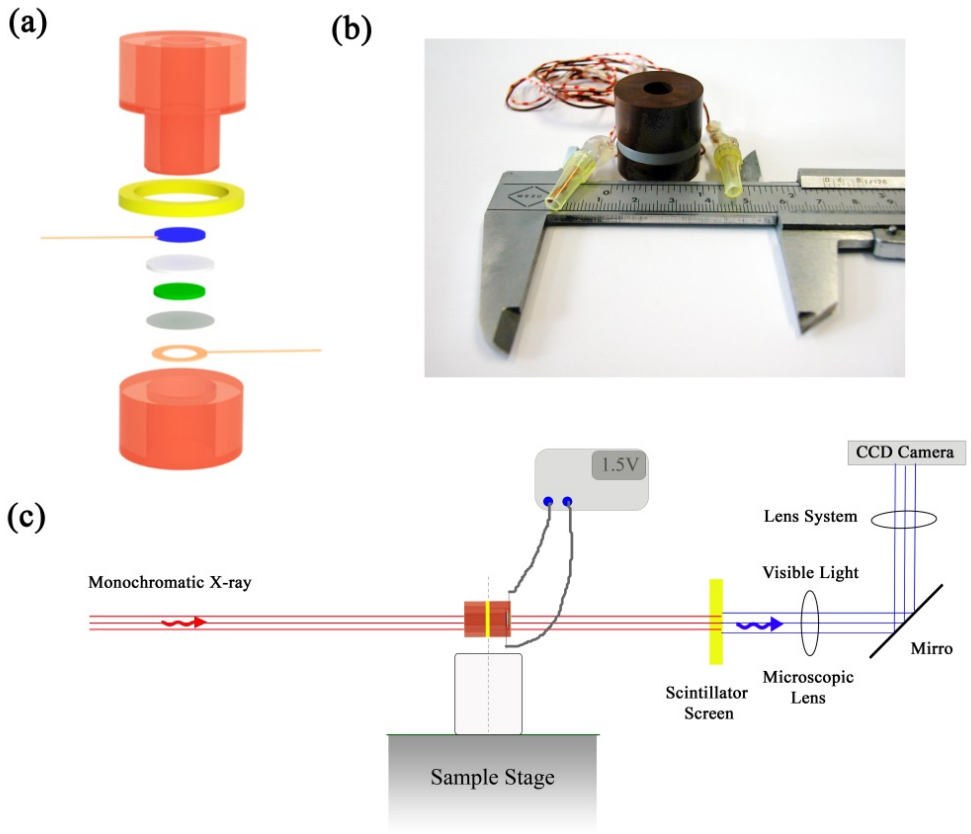

Figure 1. (a) Schematic illustration of the radiography cell used for in situ synchrotron radiography. From top to bottom: upper housing (orange), sealing ring (yellow), lithium plate (blue) with copper wire, separator (light gray), Sn/carbon/binder composite (green), titanium foil current collector (gray), annular copper current collector (copper), lower housing (orange); (b) Photograph of the radio-cell; (c) Schematic illustration of the experimental setup at the BAMline, BESSY II, Helmholtz-Zentrum Berlin, Germany. The radio-cell is arranged coaxially to the beam throughout radiography.

Synchrotron X-ray imaging is an analytical technique that maps the X-ray attenuation coefficients of samples. Since characterizations can be conducted *in situ* and non-destructively,[14] it is particularly well suited to track the morphological evolution of particles and changes of an entire electrode as a function of discharge/charge state. The presented synchrotron X-ray radiography was conducted at the BAM*line* at BESSY II, Helmholtz-Zentrum Berlin, Germany.[15] A beam energy of 17 keV was chosen for optimal beam transmission and image contrast using a double multilayer monochromator with an energy resolution of about 1.5%. A PCO4000 camera with a 4008×2672 pixel^2 CCD chip was used with optics resulting in a pixel size of 0.438 µm and a field of view (FoV) of 1.7×1.2 mm^2 (width×height). One radiographic image was acquired every 60 s at a relatively low X-Ray flux (synchrotron was operated in the single bunch mode). In order to obtain large and representative data of the de/lithiation mechanism inside the radio-cell during dis/charge process, consecutively three different regions as marked region 1-3 in Figure S1 were characterized.

All normalized projections acquired from the *in situ* radiography are shown in the Supporting Movies (SM) and Figure S3 displays an enlarged view of the pristine state of the consecutively characterized three regions. Different de/lithiation behaviors inside the multi-Sn particles battery during dis/charge process are shown in Figure 2. We track in detail structural changes of one Sn particle (green dotted circle in Figure 2A at time 00:00) during de/lithiation, representing the class of electroactive particles' evolution as a function of the dis/charge process. The location of this particle is shown in Figure S3. As can be clearly seen from the

1st row of Figure 2A, following the first lithiation (from left to right), the sharp contour of the electrochemically active Sn particle becomes progressively blurry during which its volume increases upon further lithiation. Finally, a sudden disintegration involving multiple cracks and fragments occurs and the particle resembles cauliflower-type morphology. During the 1st delithiation process, as shown in the 2nd row in Figure 2A (from right to left), the volume decreases gradually. The 3rd row in Figure 2A shows the 2nd lithiation process of this particle. It is worthy to note that compared with the 1st lithiated state, there is a limited volume expansion during the 2nd lithiation, suggesting a limited lithium uptake capability and a resultant capacity loss during the 2nd discharge. Additional evidence for Li insertion and extraction into or from the Sn particle are the changes of the histogram of transmission values in regions containing this particle as shown in Figure 3A (includes the 1st discharge, 1st charge and 2nd discharge). The rightmost peak corresponds to the weakly absorbing carbon, binder and electrolyte, the leftmost peak corresponds to the Sn particles and the changes to the middle peaks are directly related to the electrochemical evolution of Sn particle. Following the 1st lithiation process, the peak moves progressively from left to right, implying that the Sn particle is gradually transforming from the high-density Sn phase to a low-density Li_XSn phase ($1<x<4.4$).[16] During the 1st delithiation process, we find that the peak shifts gradually towards the original direction. The present demonstrations that the de/lithiation-induced volumetric expansion/contraction by Sn lattice dislocation and plastic deformation during dis/charge process are in good agreement with previous reports.[7, 17] However, it is worth noting that, neither the peak position nor the peak shape of Sn is restored to that of the original state by the end of the 1st charge process. This may stem from the incomplete delithiation and/or a significant amount of lithium trapped in the decomposed electrolyte byproducts.[18]

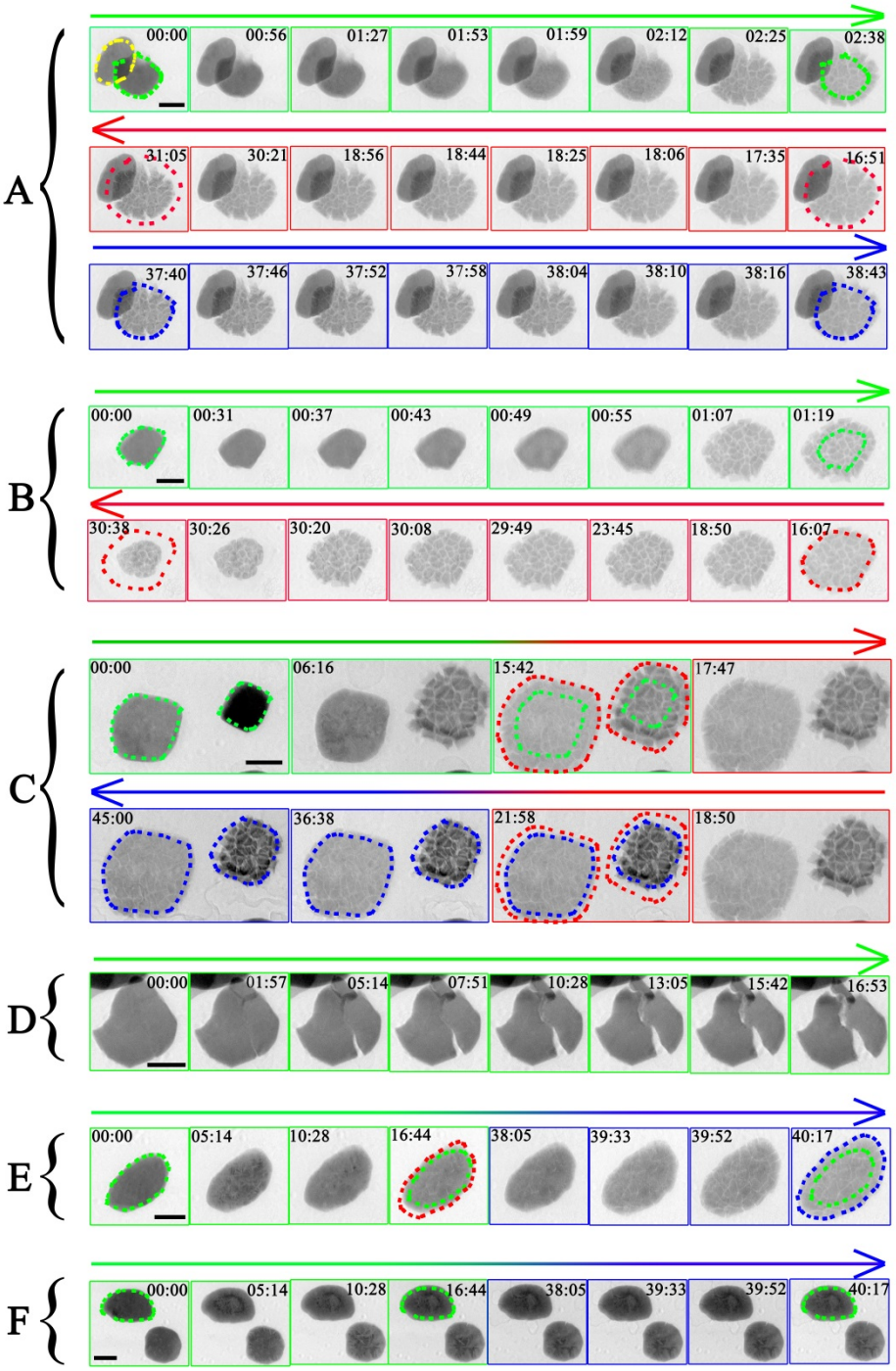

Figure 2. Demonstration of different de/lithiation behavior in the radio-cell: Panel A displays one electrochemically active and one electrochemically inactive Sn particle (green and yellow circles, respectively, in the figure labeled 00:00); Panel B shows that the time required to lithiate individual Sn particle is different from the time needed to discharge the complete battery; Panel C demonstrates the electrochemical deactivation of two Sn particles after the first cycle; Panel D shows an unexpected lithiation pathway, namely fracture instead of volume expansion occurs during first lithiation; Panel E shows one Sn particle becoming electrochemically active after the first cycle incubation period; Panel F features one Sn particle that remains electrochemically inactive after the first cycle incubation period. The locations of all the above particles are shown in Figure S3. In all figures, green rectangles mark the 1st discharge, red rectangles 1st charge, blue rectangles the 2nd discharge. Green dots encircle particles in the pristine state, red dots refer to the 1st delithiated state, blue to the 2nd lithiated state. Arrows indicate progress in time. All the scale bars shown are 50 μm long.

Surprisingly, we have also observed that many Sn particles never undergo de/lithiation during the dis/charge processes, that is to say, they are electrochemically inactive during the whole macroscopic electrode level dis/charge process, as, for example, shown in Figure 2A where the particle encircled in yellow does not show any visible evolution. Actually, the observation of electrochemically inactive Sn particles corresponds to the previous report by Wang *et al* on $LiFeO_4$ batteries, in which it was found that some particles remain intact during the whole cycle.[19] In another study on NiO electrodes by He *et al*, it was found that not all the NiO nanosheets can be reduced even as the voltage dropped to zero against Li^+/Li.[20] These recent investigations of the locally microscopic inhomogeneous electrochemical reaction with respect to the macroscopically and electrode level electrochemical performance suggest that the electrochemically driven reactions are hardly homogeneous in a commercial LIB due to the complex electrode structure and the complicated interactions.[21] The unexpected locally inhomogeneous de/lithiation behavior amongst multiple-Sn particles could have two side effects. On the one hand, the electrochemically inactive Sn particles are believed to substantially decrease the energy density due to the inefficient utilization of loaded active materials.[22] On the other hand, the inhomogeneous electrochemical reactions suggest that the overall dis/charge current is heterogeneously distributed in the electrode, that is to say, only the electrochemically active Sn particles carry the current.[9] More specifically, we have calculated the time required to lithiate the electrochemically active Sn particle shown in Figure 2B in the 1^{st} lithiation process to be approximately 1 h. In contrast, the time required to discharge the whole cell is approximately 15 h. The present time difference differs from a previous demonstration and the reason may stem from the different rates subjected to the electrochemical cells.[9]

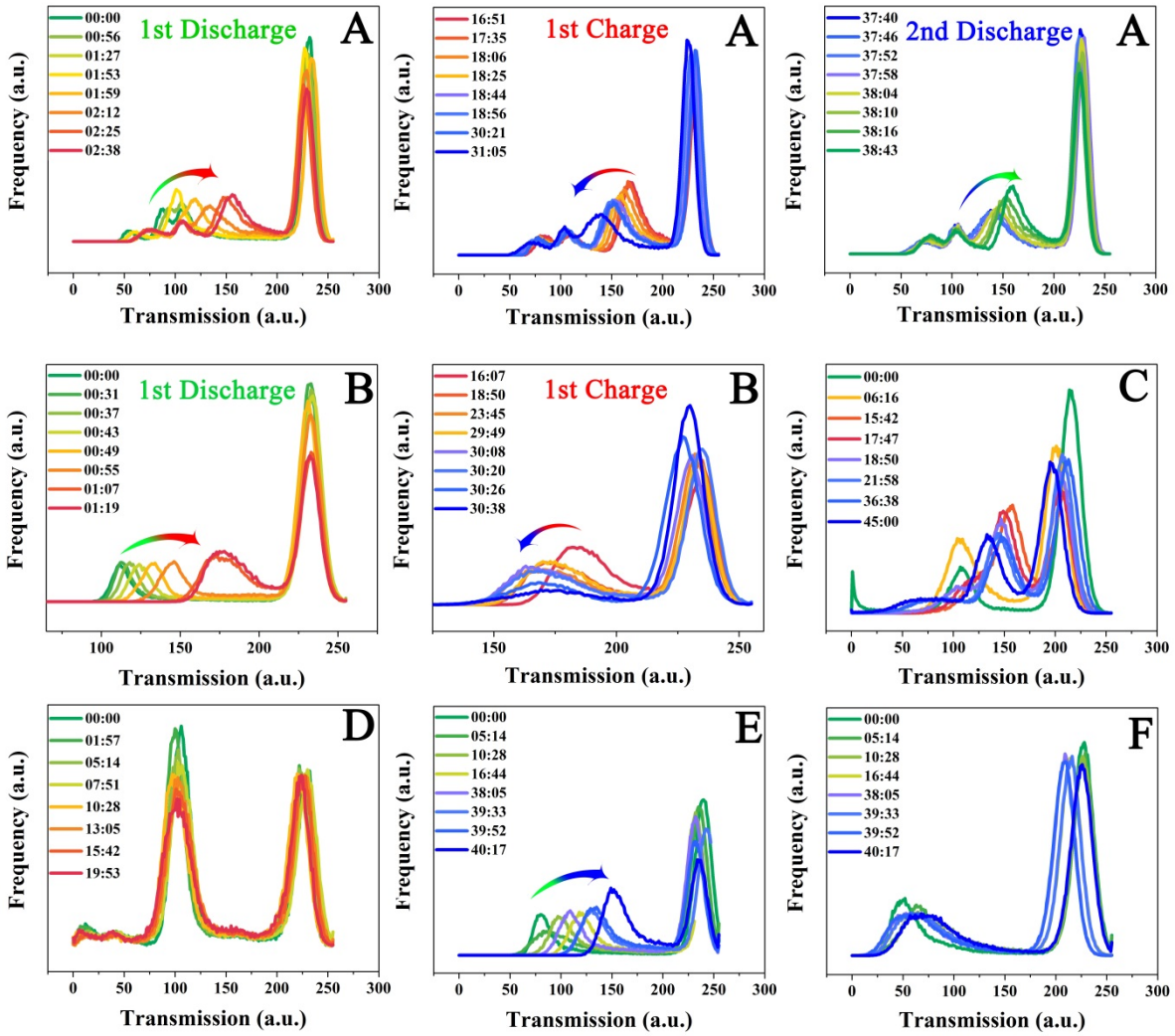

Figure 3. Transmission histograms of various regions shown in Figure 2. Color changes from green to red denote the 1st discharge, changes from red to blue the 1st charging step, changes from blue to green the 2nd discharge. Letters in each graph correspond to the letters in Figure 2 and S3.

In addition, we have also found that some Sn particles that originally participated in the de/lithiation process in the first cycle, as shown in the first row (from left to right) and the second-haft row (with time stamp 18:50 and 21:58) of Figure 2C, turned out to be electrochemically inactive during the 2nd lithiation process, as shown in the second-half row (with time stamp 36:38 and 45:00) in Figure 2C. This electrochemical deactivation process is also evident by the transmission values (barely a peak shift in the 2nd discharge, from light blue to dark blue) as shown in Figure 3C. In fact, He *et al.* proposed that the electrochemically deactivation upon silicon lithiation is caused by crystalline Li_2O, formed as a product of Li reaction with the native silicon oxide layer which partially electrically insulates the silicon particles.[23] However, as in our case, the reason may be the complex interplays between Sn particles and adjacent carbon/binder composite agents. Actually, Toney *et al.* have experimentally discovered the electrochemical deactivation of Ge particles by *in operando* transmission X-ray microscopy and they also attribute the electrochemical deactivation process to the complex interplays between Ge particles and adjacent carbon/binder agents.[24] As clearly shown in Figure 2D, during the initial lithiation process, there is a cleavage formed in this Sn particle and compared with other electrochemically active Sn particles, this Sn particle continues to further disintegrate instead of showing a

volume expansion. The underlying mechanism may be related to a partial electrical contact between this Sn particle and its adjacent carbon/binder composite. Fundamentally speaking, the lithiation process entails lithium ions and electrons simultaneously,[25] i.e., only when ionically and electronically connected to electrolyte and the electrically conducting network Sn can alloy with lithium. During the lithium uptake these electrochemically active Sn particles undergo significant volume expansion accompanied by the generation of substantial stresses[26] and the associated mechanical forces will drive local displacement and rearrangement of adjacent carbon/binder composite. Taking into account that the electron transfer between adjacent materials is based on a hopping or tunneling mechanism with a contact resistivity decaying exponentially with the gap between the contacts and that a gap of just 8-10 nm makes a contact electronically insulating,[27] it is plausible to say that the deactivation mechanism is attributed to the electric disconnection. In Figure 3D, the barely peak shifts of the disintegrated particle also suggests a limited lithiation.

Finally, we have observed that one Sn particle was partially electrochemically active in the first discharge and then turned into fully electrochemically active in the second discharge. As clearly shown in first-half row of Figure 2E, the Sn particle first undergoes a limited lithiation during the 1st lithiation step, resulting in limited volume expansion (red dot line at 16:44) and then a large volume expansion after the 2nd lithiation process (blue dot line at 40:17). This has been further demonstrated in Figure 3E, where a small peak shift from green to brawn during the 1st lithiation vs. a big peak shift from purple to blue during the 2nd lithiation. In contrast, as clearly shown in Figure 2F, another Sn particle keeps electrochemically inactive through the second discharge process and the barely shifted peaks of transmission histograms are shown in Figure 3F. Actually, He *et al.* proposed an "incubation" time to define the time required from the partial "finger" lithiation phenomenon to the fully intrinsic NiO lithiation phenomenon.[20] The incubation time observed here varies significantly from particle to particle (e.g. one particle became active after the first cycle, as show in Figure 2E; another particle might need more than one cycle to become electrochemically active, as shown in Figure 2F) and the reason may again lie in the different local environments surrounding the particles since not all Sn particles are electronically and ionically connected to electrolyte and the current collector and/or the carbon conductive network.[28] The resulting dynamic de/lithiation pathway amongst different particles can perfectly explain the previous report, in which Wang *et al.* found a monotonic specific capacity increase during cycling of a Sn/graphene half LIB.[29]

In summary, the presented study suggests that much potential benefit can be derived from experiments with electrochemical cells that can adequately simulate commercial LIBs. The firstly highlighted four cases of de/lithiation behavior in such electrochemical cells are crucially alarming because they can hardly be detected by conventional macroscopic electro-analytical or atomic single nanowire/nanoparticle characterization techniques and should draw attentions of battery research communities. In the future, examinations of electrodes prepared with different active material loading and the use of different current rates will be conducted to further obtain insights into the underlying de/lithiation mechanisms under different conditions.

Experimental Section

Sn particles were purchased from Sigma Aldrich. Conductive carbon black, polyvinylidene difluoride (PVDF), Celgard separators and lithium metal were purchased from MTI Corp. USA. N-methyl pyrrolidone solvent (NMP) and 1M $LiPF_6$ in a volume ratio (1:1) mixture of ethylene carbonate (EC) and dimethyl carbonate (DMC) were purchased from Sigma Aldrich. Titanium (Ti) foil was acquired from ANKURO Int. GmbH, Germany. The housing of the battery is made of polyamide-imide (Torlon) from McMaster-Carr Company.

The composite electrode is made of slurries of Sn: carbon black: binder in NMP with weight ratios of 60:30:10. The slurry was cast onto a 5-µm thick titanium foil. To remove the NMP, the material cast on Ti foil was dried at 60 ℃ for 15 h. Before and after casting, the Ti foil was weighed and a mass of the electrode material of 0.4 mg determined. The cell was assembled in an argon-filled glovebox with humidity and oxygen levels below 0.1 ppm. An annular copper foil was used as a current collector and the Ti foil placed on top. Lithium disks (6 mm diameter, 1 mm thick) were used as counter and reference electrodes. A polymer separator was placed between the lithium electrode and the Sn electrode. After filling with electrolyte the cell was sealed and then taken out of the glovebox to the experimental station. Different sized Sn particles will be employed to further investigate the correlation between the de/lithiation behavior and the size effect.

Cyclic voltammetry (CV) was performed by using an Ivium CompactStat station in a potential range of 0-2.5 V. Synchrotron X-ray radiography measurements were conducted in situ throughout discharge and charge of the cell. The current was calculated only on the mass of Sn. The discharge current was set to 0.75 mA/mg and after the voltage has dropped to 0 V the current was switched to 0.0225 mA/mg. The charging current was 0.015 mA/mg. There was a cell resting after the 1^{st} charge of the cell. Finally, during the second discharge the current was set to 0.0225 mA/mg.

The detector system comprised a 60-µm thick $CdWO_4$ scintillator, a microscopic optic and a pco4000 camera with a 4008×2672 $pixel^2$ CCD chip that is kept out of the direct beam by using a mirror. Radiographic images of region 1 were acquired every 60 s with 60 s exposure time. After this, regions 2 and 3 were consecutively measured. After measuring one particular region, 2 open beam images were recorded in order to normalize the acquired radiographic projections. The cell was kept discharging or charging throughout all the experiments. More information can be found in the SI.

Acknowledgements

The assistance by the beamline scientist of the BAMline, Dr. Heinrich Riesemeier, is gratefully acknowledged. We thank Norbert Beck for preparing the beamline battery. This work was sponsored by the Helmholtz Association and China Scholarship Council.

References

[1] Y. Takahashi, A. Kumatani, H. Munakata, H. Inomata, K. Ito, K. Ino, H. Shiku, P. R. Unwin, Y. E. Korchev, K. Kanamura, T. Matsue, *Nat Commun* **2014**, *5*, 5450-5457.

[2] B. Sun, K. Huang, X. Qi, X. Wei, J. Zhong, *Adv. Funct. Mater.* **2015**, *25*, 5633-5639.

[3] F. Sun, K. Huang, X. Qi, T. Gao, Y. Liu, X. Zou, X. Wei, J. Zhong, *Nanoscale* **2013**, *5*, 8586-8592.

[4] F. Sun, H. Markötter, I. Manke, A. Hilger, N. Kardjilov, J. Banhart, *ACS Appl. Mater. Interfaces* **2016**, DOI: 10.1021/acsami.1026b00708.

[5] J. Y. Huang, L. Zhong, C. M. Wang, J. P. Sullivan, W. Xu, L. Q. Zhang, S. X. Mao, N. S. Hudak, X. H. Liu, A. Subramanian, H. Fan, L. Qi, A. Kushima, J. Li, *Science* **2010**, *330*, 1515-1520.

[6] X. H. Liu, J. W. Wang, S. Huang, F. Fan, X. Huang, Y. Liu, S. Krylyuk, J. Yoo, S. A. Dayeh, A. V. Davydov, S. X. Mao, S. T. Picraux, S. Zhang, J. Li, T. Zhu, J. Y. Huang, *Nat Nano* **2012**, *7*, 749-756.

[7] L. Zhong, X. H. Liu, G. F. Wang, S. X. Mao, J. Y. Huang, *Phys. Rev. Lett.* **2011**, *106*, 248302-248306.

[8] M. Gu, L. R. Parent, B. L. Mehdi, R. R. Unocic, M. T. McDowell, R. L. Sacci, W. Xu, J. G. Connell, P. Xu, P. Abellan, X. Chen, Y. Zhang, D. E. Perea, J. E. Evans, L. J. Lauhon, J.-G. Zhang, J. Liu, N. D. Browning, Y. Cui, I. Arslan, C.-M. Wang, *Nano Lett.* **2013**, *13*, 6106-6112.

[9] Y. Li, F. El Gabaly, T. R. Ferguson, R. B. Smith, N. C. Bartelt, J. D. Sugar, K. R. Fenton, D. A. Cogswell, A. L. D. Kilcoyne, T. Tyliszczak, M. Z. Bazant, W. C. Chueh, *Nat. Mater.* **2014**, *13*, 1149-1156.

[10] T. R. Ferguson, M. Z. Bazant, *J. Electrochem. Soc.* **2012**, *159*, A1967-A1985.

[11] A. R. Benetti, J. Jacobsen, B. Lehnhoff, N. C. R. Momsen, D. V. Okhrimenko, M. T. F. Telling, N. Kardjilov, M. Strobl, T. Seydel, I. Manke, H. N. Bordallo, *Sci. Rep.* **2015**, *5*, 8972-8980.

[12] Z. Shen, Y. Hu, Y. Chen, X. Zhang, K. Wang, R. Chen, *J. Power Sources* **2015**, *278*, 660-667.

[13] N. Li, H. Song, H. Cui, C. Wang, *Nano Energy* **2014**, *3*, 102-112.

[14] D. S. Eastwood, V. Yufit, J. Gelb, A. Gu, R. S. Bradley, S. J. Harris, D. J. L. Brett, N. P. Brandon, P. D. Lee, P. J. Withers, P. R. Shearing, *Adv. Energy Mater.* **2014**, *4*, 1300506-1300513.

[15] I. Manke, J. Banhart, A. Haibel, A. Rack, S. Zabler, N. Kardjilov, A. Hilger, A. Melzer, H. Riesemeier, *Appl. Phys. Lett.* **2007**, *90*, 214102-214105.

[16] K. Eom, J. Jung, J. T. Lee, V. Lair, T. Joshi, S. W. Lee, Z. Lin, T. F. Fuller, *Nano Energy* **2015**, *12*, 314-321.

[17] X. Li, A. Dhanabalan, L. Gu, C. Wang, *Adv. Energy Mater.* **2012**, *2*, 238-244.

[18] S. P. V. Nadimpalli, V. A. Sethuraman, S. Dalavi, B. Lucht, M. J. Chon, V. B. Shenoy, P. R. Guduru, *J. Power Sources* **2012**, *215*, 145-151.

[19] J. Wang, Y.-c. K. Chen-Wiegart, J. Wang, *Nat Commun* **2014**, *5*, 4570-4580.

[20] K. He, H. L. Xin, K. Zhao, X. Yu, D. Nordlund, T.-C. Weng, J. Li, Y. Jiang, C. A. Cadigan, R. M. Richards, M. M. Doeff, X.-Q. Yang, E. A. Stach, J. Li, F. Lin, D. Su, *Nano Lett.* **2015**, *15*, 1437-1444.

[21] F. Lin, D. Nordlund, T.-C. Weng, Y. Zhu, C. Ban, R. M. Richards, H. L. Xin, *Nat Commun* **2014**, *5*, 3358-3367.

[22] W. Zhao, G. Luo, C.-Y. Wang, *J. Power Sources* **2014**, *257*, 70-79.

[23] Y. He, D. M. Piper, M. Gu, J. J. Travis, S. M. George, S.-H. Lee, A. Genc, L. Pullan, J. Liu, S. X. Mao, J.-G. Zhang, C. Ban, C. Wang, *ACS Nano* **2014**, *8*, 11816-11823.

[24] J. N. Weker, N. Liu, S. Misra, J. C. Andrews, Y. Cui, M. F. Toney, *Energy Environ. Sci.* **2014**, *7*, 2771-2777.

[25] U. Boesenberg, F. Meirer, Y. Liu, A. K. Shukla, R. Dell'Anna, T. Tyliszczak, G. Chen, J. C. Andrews, T. J. Richardson, R. Kostecki, J. Cabana, *Chem. Mater.* **2013**, *25*, 1664-1672.

[26] M. J. Chon, V. A. Sethuraman, A. McCormick, V. Srinivasan, P. R. Guduru, *Phys. Rev. Lett.* **2011**, *107*, 045503-045507.

[27] B. P. N. Nguyen, J. Gaubicher, B. Lestriez, *Electrochim. Acta* **2014**, *120*, 319-326.

[28] R. Malik, A. Abdellahi, G. Ceder, *J. Electrochem. Soc.* **2013**, *160*, A3179-A3197.

[29] C. Wang, Y. Li, Y.-S. Chui, Q.-H. Wu, X. Chen, W. Zhang, *Nanoscale* **2013**, *5*, 10599-10604.

Supplementary Information

For the normalization (N) of X-ray radiography (R), flat field (FF, without samples) and dark field images (DF, without beam) are used. The normalization process is expressed by:

$$\mathrm{N} = \frac{R - DF}{FF - DF}$$

and conducted by ImageJ.

The originally obtained radiographies are 4008 x 2627 pixels in size. For the movie, we have used Bilinear Interpolation to reduce the size. The repetition frequency of the image series is 15 fps.

Battery information

In a normal electrode, the weight ratios of active material:conductive agent:binder agent is usually set to 80:10:10[1]. In the present investigation, in order to reduce possible particle overlapping in the radiographs, a weight ratio of Sn:Carbon:Binder of 60:30:10 was used. From Figure S1 and Figure S3, we can see that the individual Sn particles can be clearly separated from one to another, thus facilitating our investigations.

The cyclic voltammetry (CV) diagram of the radio-cell is shown in Figure S2b. The cathodic peaks at around 1.0 and 0.5 V of the first scan are caused by the formation of solid electrolyte interface (SEI)[2], and the peak at 0V is due to the Li-Sn alloying reaction[2]. The anodic peaks at around 0.25V and 0.6V are due to the de-alloying of Li-Sn and the decomposition of the electrolyte, respectively[3].

SI Figure 3 shows the locations of different Sn particles displayed in Figure 2. Specifically, the electrochemically active particle is located in location A in SI Figure 3; the particle which is shown to have different lithiation time with relation to the whole battery discharge time is located in location B in SI Figure 3; the particles show electrochemically de-active processes after the first cycle are located in location C in SI Figure 3; the particle shows cleavage is located in location D in SI Figure 3; the incubation-active particle is located in location E in SI Figure 3, the incubation-inactive particles are located in location F in SI Figure 3.

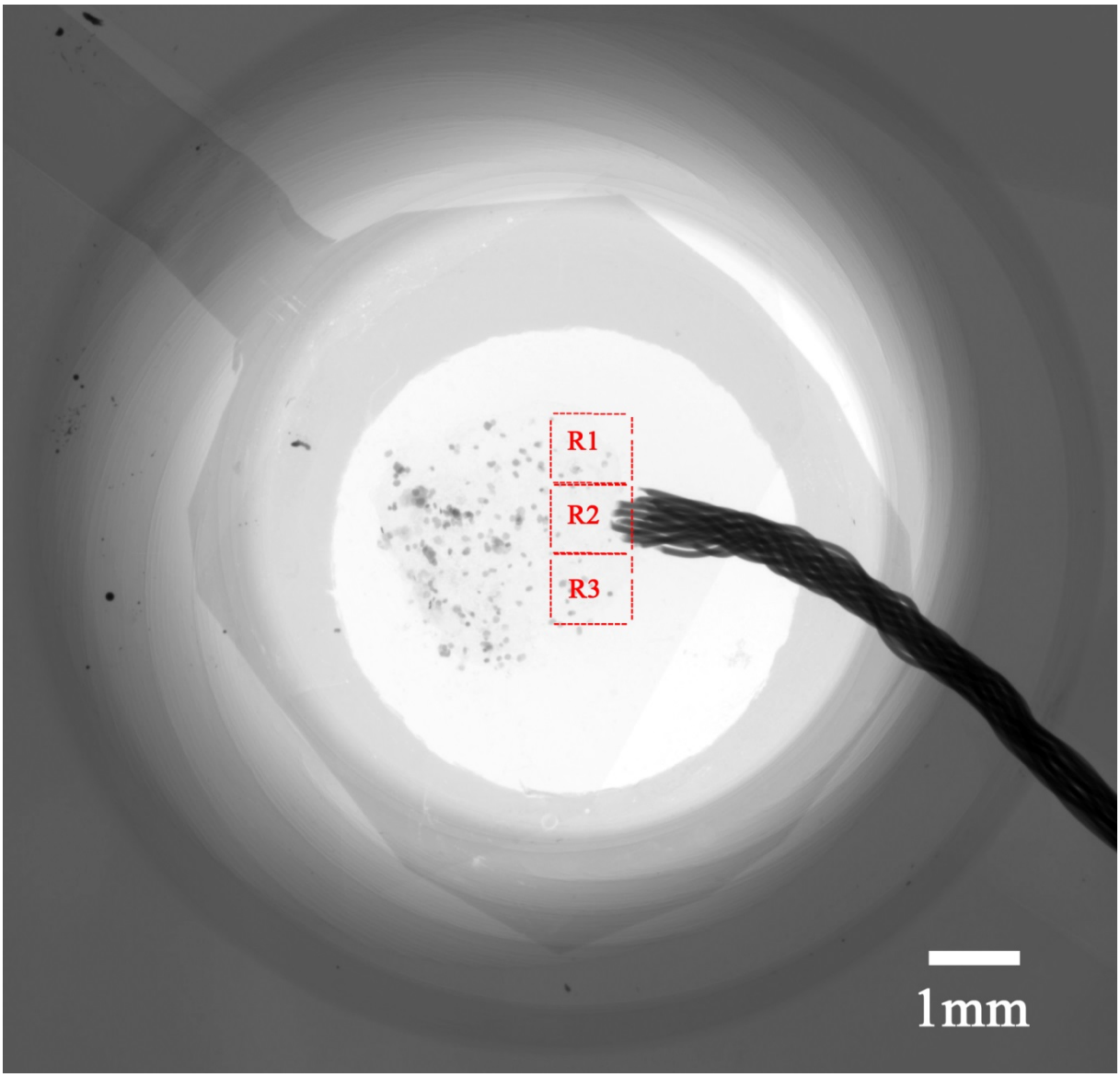

Figure S1. A projection image of the Li electrode/separator/Sn electrode assembly within the radio-cell characterized by a laboratory micro X-ray source after synchrotron X-ray measurement. The radio-cell is arranged coaxially to the beam throughout radiography. Region 1 (R1) is the region that firstly measured, after which regions R2 and R3 were acquired. The acquired images of these three images from synchrotron X-ray were composed to one image, as shown in Figure S3. Note that due to the low X-ray absorption of the radio-cell, housing, lithium electrode, separator and titanium foil are nearly invisible, only the Sn particles, the annular copper current collector and the copper wire are visible.

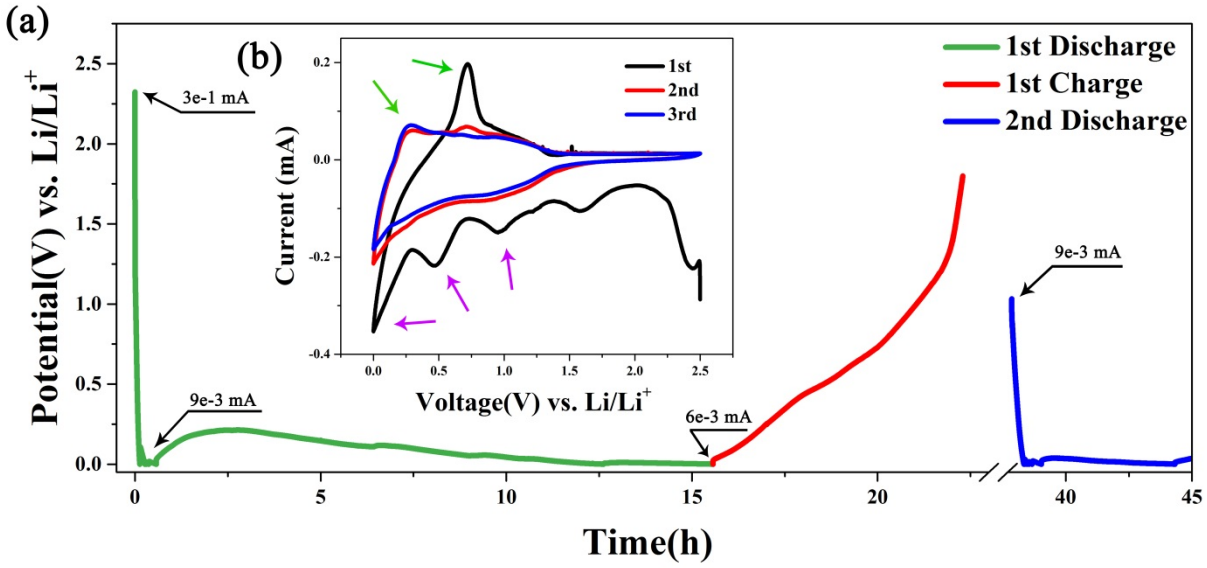

Figure S2. Electrochemical characterization of the battery: a) Discharge and charge curves of the cell. Inset figure (b): cyclic voltammetry (CV) curves scanned at 1 mV s^{-1} in the potential window 0-2.5V. Purple arrows point at the cathodic peaks, green arrows point the anodic peaks.

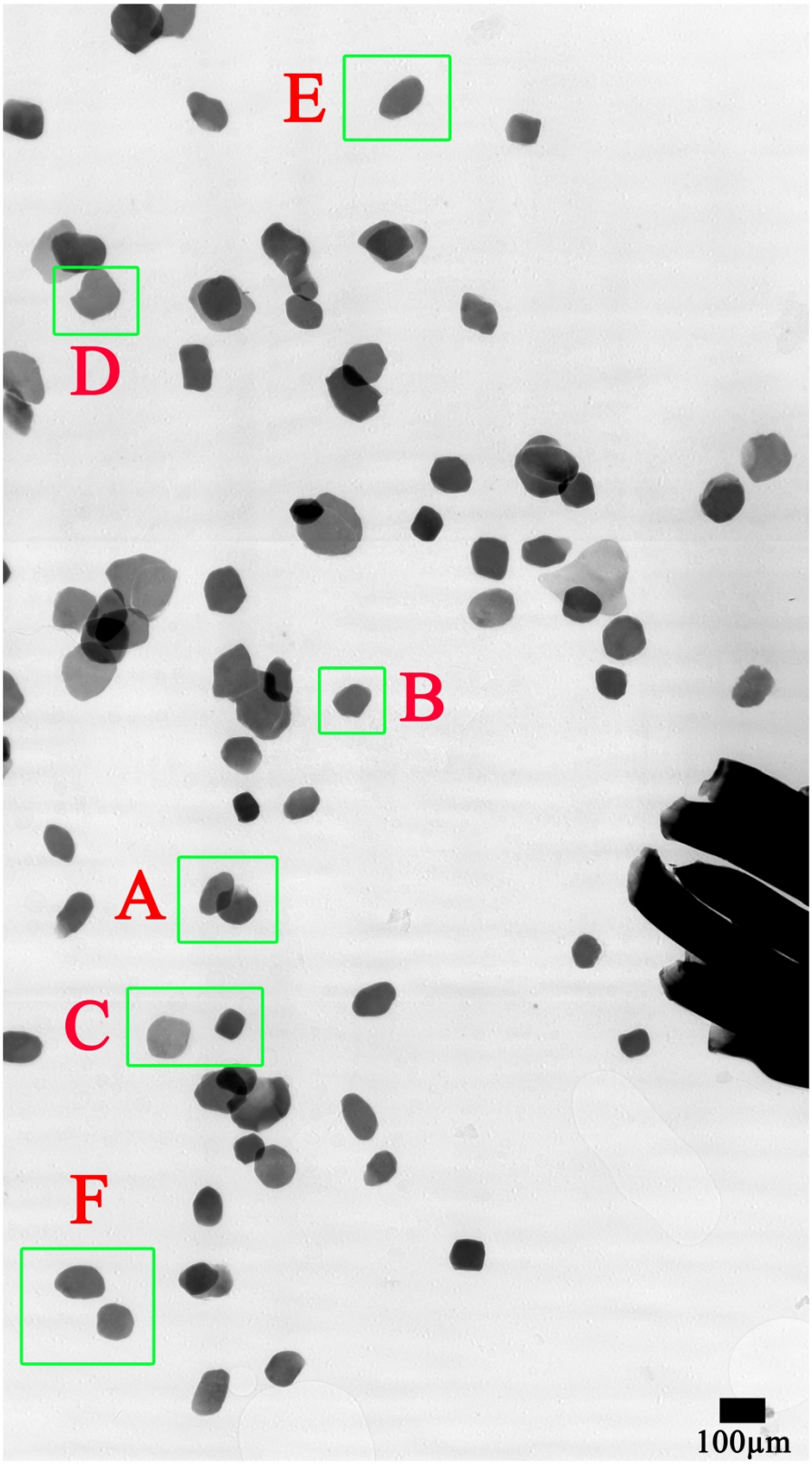

Figure S3. Locations of the particles in the electrode in the pristine state shown in Figure 2 in the main text. A: electrochemically active particles, B: particle whose lithiation time is different from the whole battery's discharge time, C: deactivated particles, D: particle hat has formed a cleavage, E: active particle after incubation, F: inactive particle after incubation.

Supplementary Movies

Position_1-Movie

Position_2-Movie

Position_3-Movie

References

[1] H. Qiao, K. Chen, L. Luo, Y. Fei, R. Cui, Q. Wei, *Electrochimica Acta* **2015**, *165*, 149-154.
[2] N. Li, H. Song, H. Cui, C. Wang, *Nano Energy* **2014**, *3*, 102-112.
[3] Z. Shen, Y. Hu, Y. Chen, X. Zhang, K. Wang, R. Chen, *J. Power Sources* **2015**, *278*, 660-667.